Volume 1 | Number 1 | Jan 2013 | Pages 1–100

RSC Advances

www.rsc.org/advances

ROYAL SOCIETY OF CHEMISTRY

ROYAL SOCIETY OF CHEMISTRY

www.rsc.org/advances

Journal Name

ARTICLE

Facile synthesis of nitrogen-doped hierarchical porous lamellar carbon for high-performance supercapacitors

Wang Yang,[ab †] Zhiling Du,[ab †] Zhipeng Ma,[b] Guiling Wang,[b] Heping Bai,[c] Guangjie Shao*[ab]

Three-dimensional (3D) interconnected N-enriched hierarchical porous lamellar carbon (NPLC) with multilevel pore structure has been fabricated by a wet impregnation method using waste nitrogen-containing mantis shrimp shell as carbon precursor and KOH as impregnation solution. The synthesized NPLC-2 shows the large surface area of 1222.961 $m^2 g^{-1}$ calculated by BET method, hierarchical porous structure analyzed by density functional theory (DFT) model, and high nitrogen content of 1.78% quantified by X-ray photoelectron spectroscopy (XPS). Moreover, NPLC-2 sample exhibits ultra-high specific capacitance of 312.62 F g^{-1} at 0.3 A g^{-1}, excellent rate capability with the specific capacitance of 272.56 F g^{-1} at 20.0 A g^{-1} and outstanding cycling stability of around 96.26% capacitance retention after 10000 cycles at a high current density of 20.0 A g^{-1}. In addition, NPLC-2 presents a high energy density of 15.05 Wh Kg^{-1} at 270W Kg^{-1}, and up to 10.12 Wh Kg^{-1} even at a large power density of 14580 W Kg^{-1}. Herein, the prepared material can be applied in high energy density and high power density demanded fields.

1. Introduction

Porous carbon is considered to be an advanced electrode material for supercapacitors owing to its high specific surface area, unique structure, strong thermal and chemical stability and simple charge storage mechanism.[1-5] The precursor source of porous carbon is various, including organics, inorganics and complex. Some reports[6-9] have successfully prepared the porous carbon using carbide and polymer as raw materials. But its cost and jeopardy were tremendous and the preparation procedure was tedious.

Recently, with the rapid development of society and the significant improvement of living standards, biological wastes are increasing. In terms of resource recycling and environment conservation, biological wastes have great potential for applications in various aspects covering energy materials and functional materials.[10-13] Compared with other resources of carbon materials, biomass materials as a green resource possess the remarkable predominance of short renewal cycle and natural texture structure, which endow them with the opportunities of reutilization in the future with resource scarcity. Due to the sustainability and economical efficiency of porous carbon production, biological materials have gradually developed into a promising raw material candidate. Huang et

al.[14] reported that hierarchical porous carbon obtained from animal bone had high surface area (S_{BET} = 2157 m^2g^{-1}) and large total volume (V_t = 2.26 cm^3g^{-1}). Sun et al.[15] revealed that porous carbon derived from coconut shell possessed a much higher specific capacitance (268 F g^{-1} at 1 A g^{-1}) than ordinary activated carbon (210 F g^{-1}) and excellent cycle durability. Additionally, different categories of biomass have their own fine texture haracteristics and natural compositions. It is supposed that the porous carbon with superior properties can be fabricated by electing appropriate biomass. Researches[16-20] showed that nitrogen-modification could optimize the structure and improve the performance of porous carbon. Therefore, nitrogen-doped porous carbon has attracted increasing attentions as an ideal electrode material for supercapacitor. White et al.[21] successfully obtained nitrogen-doped porous carbon with high surface area (S_{BET} > 300 m^2g^{-1}) and large pore volume (V_{pore} > 0.3 cm^3g^{-1}) using prawn shell as carbon resource. At the same time, the product preserved the original texture of carbon resource. In terms of the porous carbon electrode materials used for supercapacitor, the most fundamental question is its pore structure because the structure determines performance. What concerns most is exploring better parameter to supercapacitor for charge storage among pore size distribution , the pore-network connectivity and

a. State key Laboratory of Metastable Materials Science and Technology, Yanshan University, Qinhuangdao 066004, China. E-mail: shaoguangjie@ysu.edu.cn; Fax: +86-335-8061569; Tel: +86-335-8061569
b. Hebei Key Laboratory of Applied Chemistry, College of Environmental and Chemical Engineering, Yanshan University, Qinhuangdao 066004, China
c. College of Real Estate, Beijing Normal University, Zhuhai 519000, China
† Wang Yang and Zhiling Du contributed equally.

doping of carbon materials .Therefore, we plan to select a kind of special biomass waste to synthesize an electrode material for supercapacitors with better pore structure as well as superior electrochemical performance.

Mantis shrimp shell enriches with abundant chitin (poly-β (1,4)-N-acetyl-2-amino-2-deoxidation-D-glucose) and natural inorganic calcium salt which can act as natural template in preparing porous material. Herein, we prepared a nitrogen-doped hierarchical porous lamellar carbon via a facile wet impregnation method using mantis shrimp shell as nitrogen-rich carbon precursor and KOH as auxiliary pore-forming agent. The obtained material exhibits an ultra-high specific capacitance of 312.62 F g^{-1} at 0.3 A g^{-1}, an excellent rate capability with the specific capacitance of 272.56 F g^{-1} at 20.0 A g^{-1}, which are superior to other reported literatures.[14-15] This is attributed to the reasonable microstructure, including the appropriate aperture size, hierarchical pore size distribution, three-dimensional pore structure and the nitrogen doping. Such result give us certain inspiration and references as to design and optimize the structure of porous carbon electrode material for supercapacitor.

2. Experimental

2.1. Chemicals

In this experiment, the used chemicals KOH and HCl are of analytical grade and they were used directly as received without any further processing. Deionized water as a cleaning agent was used in the whole experiment.

2.2. Preparation of NPLCs

NPLC materials were synthesized via alkali solution impregnation method using N-enriched mantis shrimp shell as a sustainable and economic carbon precursor and KOH as impregnation solution. In the pretreatment procedure, 15.0 g of the washed mantis shrimp shell was mixed with 50 ml of 10 wt% KOH solution (ca. 5.0 g KOH), and the mixture was oscillated for 3 h by ultrasonic cleaner to assist KOH in soaking into the internal structure of mantis shrimp shell. Then the mixture was evaporated at 80℃ overnight in oven to obtain impregnated carbon precursor. Subsequently, the impregnated product was transferred into three ceramic crucibles and was carbonized in a furnace at the desired temperature of 700℃ (NPLC-700), 750 ℃ (NPLC-750) and 800 ℃ (NPLC-800) respectively for 1 h under inert N_2 atmosphere. Then the calcined products were etched with 15 wt% HCl, filtrated by vacuum pump and rinsed with deionized water until it became neutral. Finally the products were dried at 80℃ for 12 h to obtain the final samples of NPLC-700, NPLC-750 and NPLC-800, which are labeled as NPLC-1, NPLC-2 and NPLC-3, respectively.

2.3. Structure Characterization

The structures of as-prepared NPLCs were characterized by X-ray diffraction (XRD) on a Rigakud/MAX-2500/pc X-ray diffractometer with Cu Kα radiation.The Raman spectra were recorded on a Horiva (LabRam HR-800) spectro-meter (532nm,50mW excitation laser). Field-emission scanning

electron microscope (FE-SEM, Hitachi Modle S-4800, KV) and transmission electron microscope (TEM, JEM2010) were employed to observe the morphology and microstructure of the materials. Fourier Transform Infrared Spectroscopy (FTIR) was used to analyze the surface functional groups on a Nicolet IS fourier transformation infrared spectrometer with the wave number range of 400-4000 cm^{-1}. Elemental quantitative analysis was achieved using X-ray photoelectron spectroscopy (XPS) with a Kratos XSAM-800 spectrometer with Al Kα radiation source. High-resolution spectra of the individual elements were acquired with the analyzer pass energy set at 20 eV. The pressure of the vacuum system was set at 1×10^{-9} during all XPS operation. N_2 sorption isotherms were carried out to analyze the porous structures of the samples using a NOVA instrument (Quantachrome Instruments version 10.01). The specific surface area was calculated by BET (Brunauer-Emmett-Teller) method in the relative pressure range of 0.04-0.20. The pore volume and pore size distributions (PSDs) were obtained using the density functional theory (DFT) model from the adsorption branches of isotherms.

2.4. Electrochemical characterization

The electrochemical characterizations were carried out using a three-electrode system in 6 M KOH electrolyte. Hg/HgO electrode and active carbon electrode were used as the reference electrode and as the counter electrode, respectively. To prepare the working electrodes NPLCs, acetylene black and polytetrafluoroethylene (PTFE) binder were mixed at a weight ratio of 80:15:5 into uniform slurries which were coated the slurry on current collectors of 1 cm^2 nickel foam in area, and dried at 80℃ for 12 h. The total mass loading of each NPLC-based electrode was 3 mg in which the active material was 2.4 mg. The fabricate electrodes were pressed at 4 MPa pressure for 30 s, and marinated in 6 M KOH electrolyte for 24 h.

CHI660E electrochemical workstation (Chenhua, Shanghai China) was employed to carry out the cyclic voltammetry (CV) and electrochemical impedance spectroscope (EIS) tests. The CV was tested at various scanning rates of 5, 20, 50 and 100 mV s^{-1}. The frequency range for the EIS measurement was from 1 mHz to 1 MHz. The galvanostatic charge-discharge measurement was recorded on a NEWARE auto-cycler and the potential window was -1.0 to 0.11 V. The specific gravimetric capacitance of the working electrodes was obtained from the galvanostatic discharge process via $C_{gd} = I\Delta t/(m\Delta V)$, where I (A) is the discharge current, Δt (s) is the discharge time, ΔV (V) is discharge voltage change excluding the IR drop during discharge process, and m (g) is the mass of the active material for each electrode. The specific capacitance could also be calculated from the CV curve via $Ccv = \int_{V_a}^{V_c} IdV/[mv(V_c - V_a)]$, where Ccv (F g^{-1}) is the specific capacitance, I (A) is the discharge current, m (g) is the mass of active material of working electrode, v (V s^{-1}) is the scan rate, and Va and Vc represent the low and high potential limits from CV test, respectively. Particularly, the symmetrical total cell was used to analyze the power and energy density in a symmetrical two-

Journal Name ARTICLE

electrode system. The energy density was calculated using the equation of $E = \left(C_{cell} V^2 \right)/2$, where Ccell (F g^{-1}) is the total cell specific capacitance and V (V) is the cell-operation potential. The average power density was calculated via $P = E/\Delta t$, where E is the energy density and Δ t is the discharge time.

● Mantis shrimp shell   ● KOH   ● Carbon
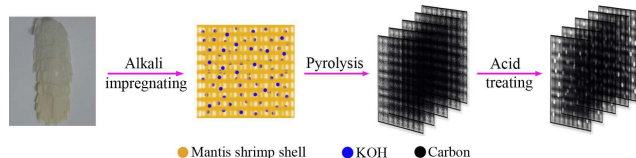
Scheme 1 Schematic preparation procedure of 3D interconnected NPLCs
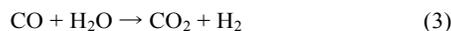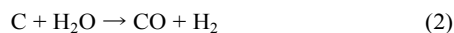
3. Results and discussion

3.1. Structure and morphology analysis

XRD and Raman spectra are carried out to analyze the structure characteristics of the prepared materials. Fig. 1a presents the XRD patterns of NPLCs synthesized at 700 ℃, 750 ℃ and 800 ℃, respectively. An inconspicuous peak locates at near 43° corresponding to a superposition of the graphitic (101) and (100) planes and a broad humps positions at 2θ = ~ 23° which is attributed to the graphitic (002) reflection.[22] The peak at around 23° shifts to lower diffraction angle in comparison to the ideal graphitic (002) peak at 26°, indicating that the interlayer spacing (002) of NPLCs is larger than the ideal value of 0.34 nm for the ordered graphite (002), and the materials present amorphous structure.[23] Moreover, it can be detected that the humps shift to the lower diffraction angle with increasing calcination temperature. It is speculated that the increasing interlayer spacing is caused by the higher gas pressure during the reaction with increasing temperature. The Raman spectra present the characteristic bands of D (defect) band, G (graphite) band and 2D band, as shown in Fig. 1b. The D band centered at 1350 cm^{-1} is related to defects in carbon materials (sp^3-coordinated), and the G band at 1590 cm^{-1} corresponds to the ordered graphitic structure of carbon (sp^2-coordinated).[24] The relative intensities (ID/IG) can be used to evaluate the orderly degree of atomic arrangement of carbon. The ID/IG value of NPLCs changes from 0.916 to 0.968 and 2D peak also gets weak with the temperature increasing from 700 ℃ to 800 ℃,

suggesting the increase of amorphous degree, which is consistent with the XRD analysis.

Fig. 2a-d shows the SEM and TEM images of NPLC-2 at different magnifications. As seen from SEM images of Fig. 2a-b, the sample has a typical 3D web-like porous structure, and the pores with different sizes play different roles in optimizing the electrochemical properties of the product. The numerous pores originated from the etched natural mineral salt of CaCO$_3$, the corrosive action of KOH and the decomposition of chitin during pyrolysis process. TEM images in Fig. 2c-d show a layered structure with abundant hierarchical porosity of NPLC-2. The porous lamellar structure can provide more accessible paths which are favorable for the fast charge transfer and a higher surface area contributing to more charge absorption sites. It is deduced that the porous lamellar structure is closely related to the natural skeleton and chemical component of mantis shrimp shell. More importantly, KOH impregnated into its internal structure plays a significant role in the formation of porous graphite-like lamellar structure. A possible action mechanism is proposed in Scheme 1 with the following illustrations.

Firstly, KOH is decomposed into K$_2$O and H$_2$O at the temperature of 400 ℃ (Eq. (1)).[25] The generated H$_2$O reacts with C resulting in the consumption of carbon according to Eq. (2). Simultaneously, the reaction of Eq. (3) and Eq. (4) are happening.

$$2KOH \rightarrow K_2O + H_2O \qquad (1)$$
$$C + H_2O \rightarrow CO + H_2 \qquad (2)$$
$$CO + H_2O \rightarrow CO_2 + H_2 \qquad (3)$$
$$K_2O + CO_2 \rightarrow K_2CO_3 \qquad (4)$$

When the calcination temperature exceeds 700 ° C, K$_2$CO$_3$ can be highly decomposed (Eq. (5)).[2] Consequently, the reaction product of CO$_2$ and K$_2$O are reduced by carbon according to Eq. (6) and Eq. (7).

$$K_2CO_3 \rightarrow K_2O + CO_2 \qquad (5)$$
$$CO_2 + C \rightarrow CO \qquad (6)$$
$$K_2O + C \rightarrow 2K + CO \qquad (7)$$
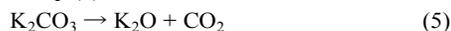
It is notable that considerable gas and pores are introduced in the activation-KOH process, some of which are formed in the internal texture. The pressure in the interior of the precursor
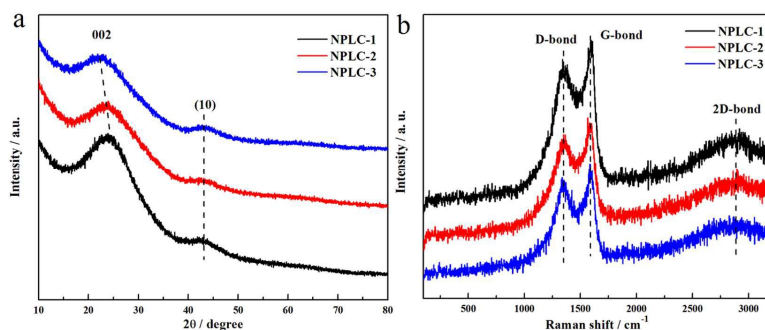

Fig. 1 (a) XRD patterns and (b) Raman spectra of NPLC-1, NPLC-2, and NPLC-3, respectively
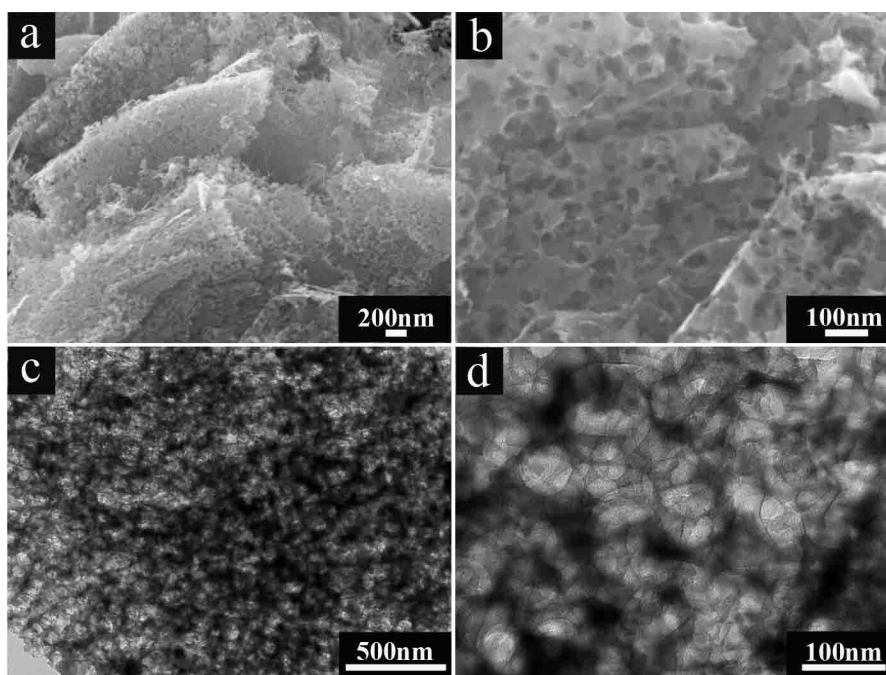
Fig. 2 TEM images and SEM images of NPLC-2: (a-b) SEM images; (c-d) TEM images

grows as the reaction progress. As a result, natural elaborate texture of raw material expands to form porous lamellar structure during carbonization process. Certainly, the natural template of inorganic salt and the release of small molecules of CO_2, H_2O and H_2 have a vital impact on the formation of pore structure.

Large surface area and favorable pore size distribution are known as significant factors in advanced electrode material for supercapacitors. In this test, the nitrogen adsorption-desorption test is carried out to investigate the textural properties, and the density functional theory (DFT) mode is used to analyze the pore volume and pore size distribution. The main parameters of pore structure of NPLC are listed in Table S1. The as-obtained NPLC materials show a cross between type-I and type-IV N_2-adsorption isotherms as depicted in Fig. 3a, which implies that the NPLC samples enrich with abundant micropores and mesopores. Obviously, the isotherms of NPLCs present H_4 hysteresis loops at relatively high pressure section of above 0.9 P/P0. The result indicates that pores with narrow and slit-like shape exist in NPLC materials,[26] which is consistent with the result of TEM. Fig. 3b demonstrates that the hierarchical pores with diameters 3 nm, 12 nm, 14 nm, 17 nm and less than 2 nm exist in the fabricated materials, indicating the coexistence of micropores and mesopores in the carbon. Additionally, Fig. 3b reveals that, with the increased temperature from 700 ° C to 800 ° C, the amount of micropore is decreasing and that of different levels of mesopores is increasing. The surface areas of the samples are calculated by general BET method and the values of NPLC-1, NPLC-2 and NPLC-3 are 853.195 m^2g^{-1}, 1222.961 m^2g^{-1} and 1329.112 m^2g^{-1}, respectively. The increase in the surface area with higher calcination temperature is because the increasing degree of the mesopores is higher than the decreasing degree of the micropores. It has been proved that the micropores (< 2 nm) contribute to the large surface area which leads to the high specific capacitance.[27] Moreover, the small mesopore of about 3 nm can accelerate the electrolyte ion transfer and the large mesopore (> 10 nm) could store electrolyte standby for fast electrochemical reaction.[28]

FTIR is taken for qualitative analysis of chemical constitution of NPLCs, as shown in Fig. 4. The typical peak positioned at 3430 cm^{-1} is assigned to the O-H stretching vibration stemming from H_2O and the three peaks at 2970 cm^{-1}, 2920 cm^{-1} and 2850 cm^{-1} relate to the stretching vibration of C-H bond. The sharp absorption peak observed at 1630 cm^{-1} is attributed to the stretching vibration of C=X (X=C, N, or O),20 while the distinct peaks at 1380 cm^{-1}/1270 cm^{-1} are identified as C-N vibration modes.[8] In addition, the other peaks are centered at 1050 cm^{-1} (the C-N bending vibration),[29] 1130 cm^{-1} (the C-O stretching vibration) and 877cm^{-1}/669cm^{-1} (N-H out-of-plane deformation vibration).[30]The above results confirm that the derived-biomass nitrogen-doping carbon has been synthesized.

To quantify the heteroatoms enriched in the as-synthesized carbon material, the XPS technique is employed, as shown in Fig. 5. It can be observed that NPLCs are enriched with nitrogen and oxygen elements, which can boost electrochemical performances including introducing additional pseudocapacitances and enhancing interface wett-
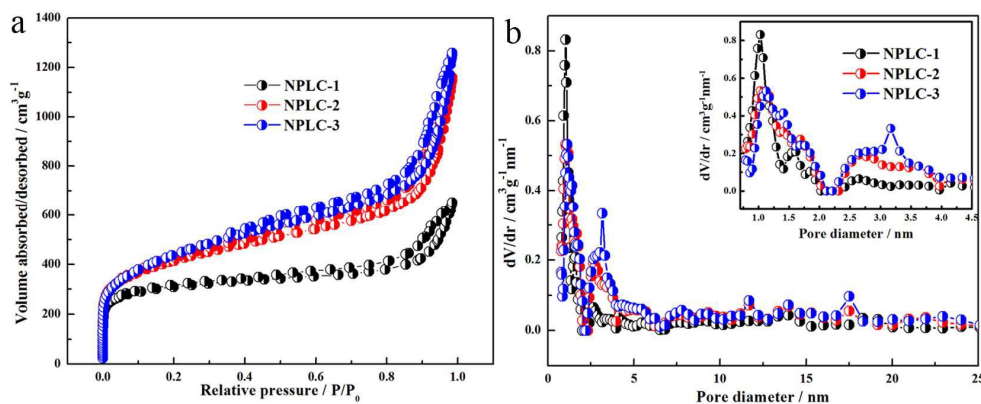
Journal Name

ARTICLE

Fig. 3 Nitrogen sorption isotherms (a) and pore-size distributions (b)

ability. The element compositions of the NPLCs are determined by XPS measurement and the content of different elements are listed in Table S1. The N content of the prepared carbons decreases from 1.99% to 0.81% with the increase of temperature. Apparently, the O content increased first increases from 6.77% to 19.21% and then decreases to 10.56%, which is due to the harsh redox reactions between the potassium compounds and carbon at 750 ℃ , and when temperature continue increases ， the oxygen containing functional groups will be reduced . Fig. 5a shows that the XPS curves of NPLCs consist of three obvious peaks of C1s (284.0 eV), N1s (400.0 eV), and O1s (532.0 eV), which accords well with the FTIR result. The nitrogen atoms in different chemical environments respectively play their own roles. The high-resolution of N1s is used to analyze the types of nitrogen species and the curve-fitting method is carried out by XPS peak-fit software. It is seen that the N1s spectra of the as-prepared carbon materials is divided into three typical component peaks including N-6 (pyridinic, 398.4 eV), N-5 (pyrrolic/pyridine, 400.1 eV) and N-Q (quaternary, 401.0 eV), as described in Fig. 5b-d. The relative content of each nitrogen type is listed in Table S1. The percentages of N-5, N-6 and N-Q range from 79.01% to 44.69%, 16.68 to 17.49.% and 4.31 to 37.82% of total nitrogen content with increasing calcination temperature. It is noticeable that the N-5 content decreases, while the N-6 and N-Q content increases. Studies found that N-5 and N-6 could enhance the capacitance performance by producing pseudocapacitance and they are situated at the edges of graphite-layer, while N-Q located at both the centre and the edges of graphite-layer could facilitate the fast transfer of electrons and ions by increasing the electronic conductivity of the as-obtained materials and improve the wettability of interface between the electrode materials and the electrolyte.[31]

Fig. S1 clearly presents the structure mode of different types of nitrogen atoms in carbon matrix. In a word, the nitrogen-doping porous carbon material originated from mantis shrimp shell has been successfully fabricated and it has a broad application prospect in various fields such as adsorption, hydrogen storage battery and supercapacitor thanks to its porous structure, high specific surface area, definite nitrogen content as well as good electrochemical characteristics which will be described below.
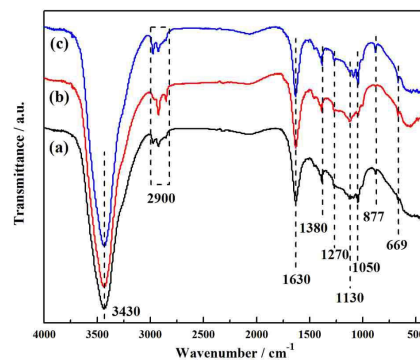

Fig. 4 FTIR spectra of as-prepared carbon materials: (a) NPLC-1; (b) NPLC-2; (c) NPLC-3

3.2. Electrochemical behavior

To investigate the causality relationship of the sample microstructure and its electrochemical performance, cyclic voltammetry (CV) measurement was carried out in a three-electrode configuration in 6M KOH. Fig. 6a presents the CV graphs of NPLCs synthesized at the different temperatures of 700 ° C, 750 ° C and 800 ° C at a scan rate of 50 mV s^{-1}. The CV curves appear rectangular with broad humps at relatively low potential, and the hump becomes inconspicuous with increasing calcination temperature, as shown in Fig. 6a. It

means that the specific capacitance of NPLCs includes in EDLC and pseudocapacitance, but the contribution of pseudocapacitance decreases with the enhanced calcination temperature due to the loss of nitrogen atom at relatively high temperature, which is accordant with XPS analysis. Moreover, it can be observed that the specific capacitance of NPLC-2 is superior to the other samples and its specific capacitance reaches up to 280.93 F g^{-1} at 50 mV s^{-1}. Fig. 6c reveals the CV curves of NPLC-2 with a typical rectangular shape at different scan rates. Even at high scan rate of 200 mV s^{-1}, the CV curve still retains ideal rectangular shape, indicating the excellent capacitive behavior of NPLC-2 with fast charge and discharge process due to the favorable pore size distribution providing short and unresisted ion diffusion paths. The CV curves display fast capacitance response at switching potentials, which means that the electrical double layer can be re-organized rapidly when the potential changes.[32] Furthermore, an obvious hump gradually appears at the potential below -0.35 V and a deviation from perfect rectangular shape is more apparent with increasing scan rate.It certifies that the capacitance of the as-obtained material contains not only EDLC but also pseudocapacitance It certifies that the

capacitance of the as-obtained material contains not only EDLC but also pseudocapacitance that which results from the produced nitrogen. It is calculated that NPLC-2 has a considerably high specific capacitance of 332.71 F g^{-1} at 5 mV s^{-1} and the capacitance still keeps up to 225.21 F g^{-1} even at a relative large scan rate of 200 mV s^{-1}, as shownin Fig. 6d, manifesting the superior rate capability. As known from pore analysis, numerous micropores indwell in NPLC-2 and they can furnish abundant charge absorption sites which improve capacitance property. Additionally, the small mesopore (ca. 2-4 nm) and the relatively big mesopore (centered at 12 nm, 14 nm, 17 nm) provide open routes for rapid ion diffusion as well as storage bank of electrolyte ions for seasonable supplement of charges. Therefore, NPLC-2 exhibits ultra-high specific capacitance and prominent rate capability of all.

To further investigate the electrochemical properties of the samples, galvanostatic charge-discharge was conducted, as shown in Fig. 6b. The charge-discharge curves of NPLCs are almost linear and with good symmetry, revealing the nice capacitive ability and high discharge efficiency, and that minor distortion is generated by the doped nitrogen atom.
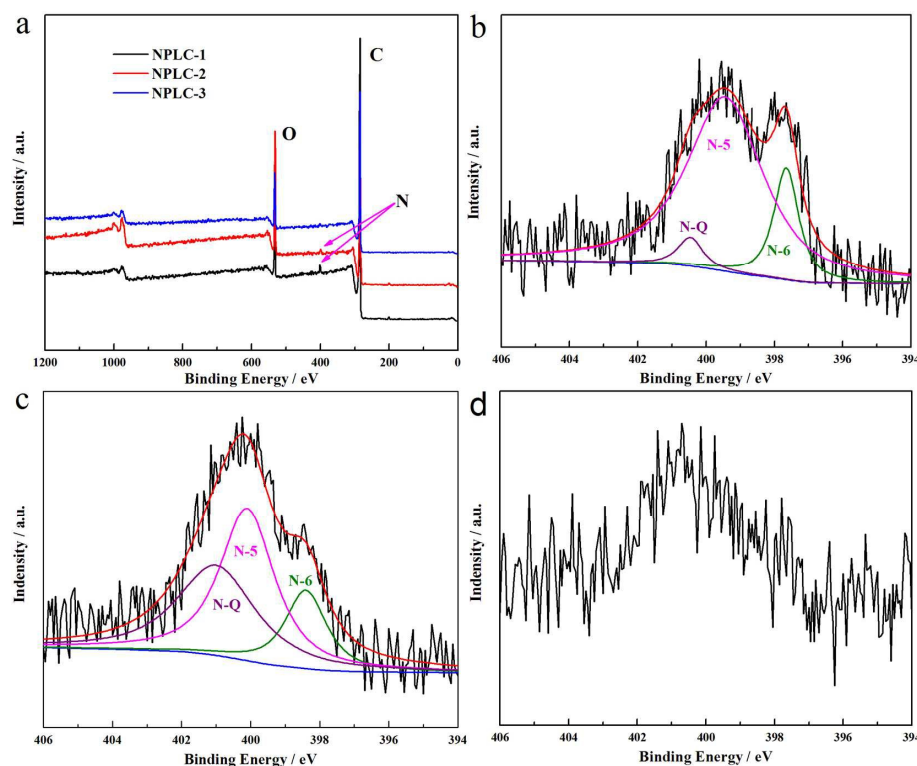

Fig. 5 XPS spectra of NPLCs (a) and N 1s XPS spectra: (b) NPLC-1; (c) NPLC-2; (d) NPLC-3 (pyridinic (N-6), pyrrolic/pyridone (N-5) and quaternary (N-Q))

Besides, the discharge time of NPLC-2 is the longest among all the samples which displays the fact the specific capacitance of NPLC-2 exceeds that of the other samples. Fig. 6e shows the V-t graphs of NPLC-2 with increasing current density from 1.0 to 20.0 A g^{-1}. From the intersection of the discharge curve branch and the horizontal axis, it can be seen that the discharge time decreases with the increase of current density

due to the presence of internal impedance from NPLC-2. Fig. 6f demonstrates that the as-obtained material has remarkable specific capacitance and superior rate capability. Its specific capacitance is up to 312.62 F g^{-1} at 0.3 A g^{-1} and still remains 272.56 F g^{-1} at a high current density of 20.0 A g^{-1} (ca.87.16% of capacitance retention). The galvanostatic charge-discharge analysis is consistent with the result of CV.

The cycle durability occupies a vital position in practical application and it is explored in detail. Fig. S2 shows the cycle life trace of the obtained samples at a current density of 20 A g^{-1}. It can be seen that all the samples display outstanding cycle durability. The specific capacitance of NPLC-2 maintains 262.37 F g^{-1} even after 10000 cycles (ca 96.26% of

capacitance retention), as shown in Fig. 6g. In addition, the coulombic efficiency of NPLC-2 is near 100% which is due to the rapid absorption and desorption of ions in the interior walls of the pores as well as the reversible chemical modification of N-functional group.
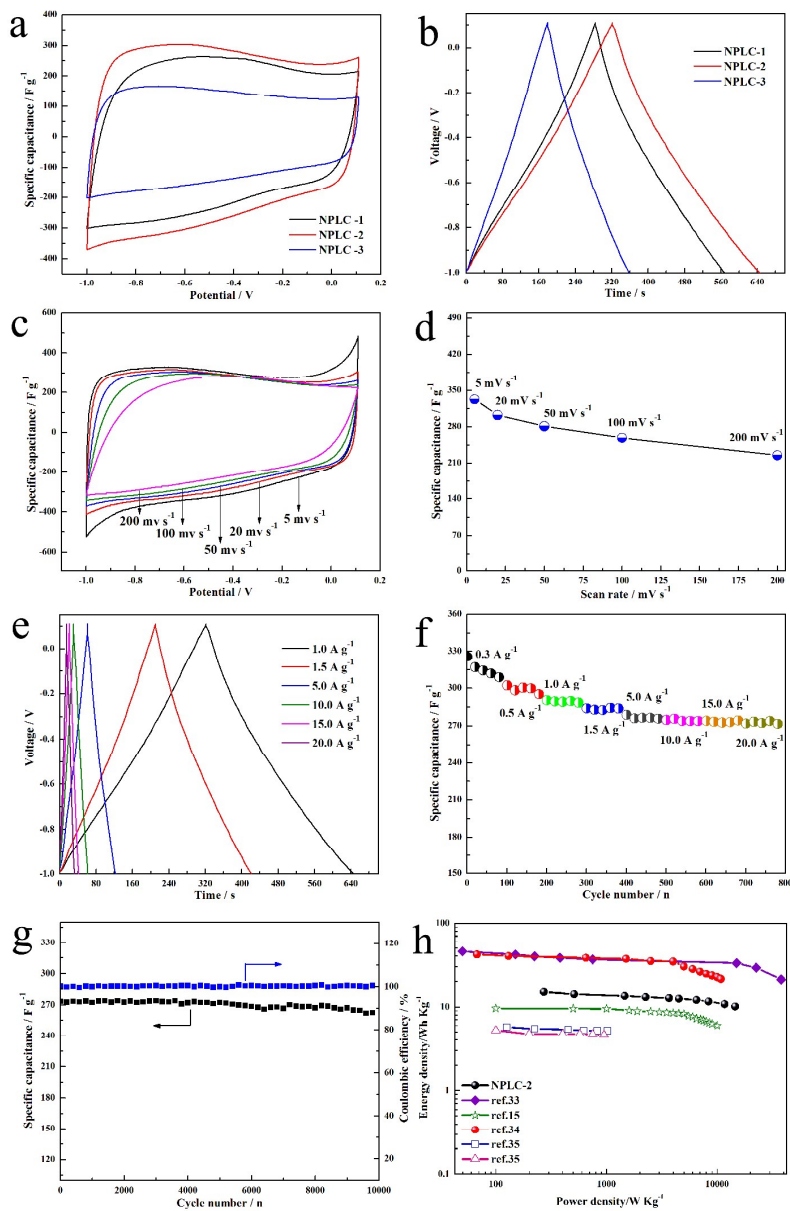

Fig. 6 Electrochemical properties of NPLCs: Electrochemical properties of (a-b) NPLCs and (c-f) NPLC-2 in a three-electrode system: (a) CV cuves at the scan rate of 50 mV s^{-1}; (b) Galvanostatic charge-discharge curves measured at a current density of 1.0 A g^{-1}; (c) CV curves at different scan rates; (d) Specific capacitance calculated by CV curves at different scan rates; (e) Galvanostatic charge-discharge curves at different current densities; (f) Specific capacitance calculated by discharge curves at various current densities; (g) Cycling life and coulombic efficiency curves of NPLC-2 tested at a current density of 20 A g^{-1} in a three-electrode system; (h) Ragone plot of porous carbon materials that can be found in the literature and NPLC-2.

Energy density and power density were performed by a two-electrode system in 6 M KOH, Fig. 6h. provides a comparison of the power and energy characteristics of the NPLC-2-based supercapacitors with those porous carbon materials that can be

found in the literature.[15,33,34,35]NPLC-2 exhibits a high energy density of 15.05 Wh Kg^{-1} at 270 W Kg^{-1}, and still retains 10.12 Wh Kg^{-1} at a large power density of 14580 W Kg^{1}. It indicates that the prepared NPLC-2 has high energy density

and power density. Generally, the superior electrochemical capability is closely related to the fine microstructure with

connectivity of pore in 3D level, large surface area, definite nitrogen content and hierarchical porous size distribution.
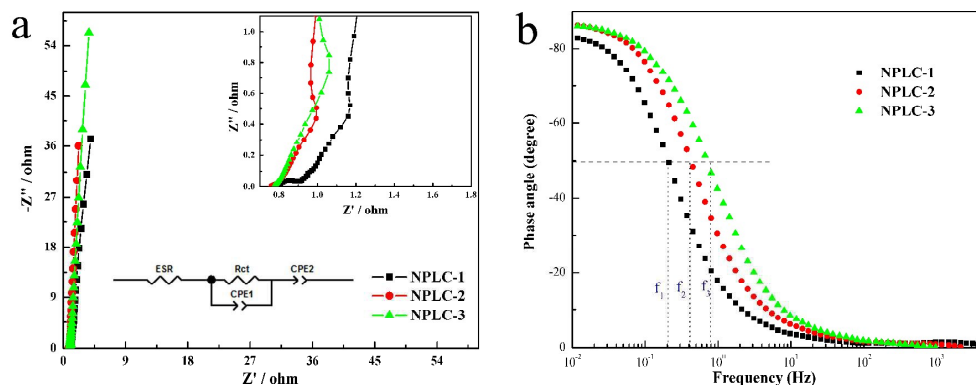

Fig. 7 (a) Nyquist plots (the inset shows amplified part of Nyquist plots), and (b) Bode plots of NPLCs

The following EIS test is to investigate the resistance and the capacitive property of the prepared samples. Fig. 7a shows that the plots of NPLC-2 and NPLC-3 at low-frequency region are more perpendicular to the real axis than that of NPLC-1, which illustrates NPLC-2 possesses the optimal capacitive behavior. The inset of Fig. 7a demonstrates that the each Nyquist plot contains three segments, including a clear semicircle, a small slop line and a large slop line. In comparison, the semicircle at the high-frequency region becomes inconspicuous with increasing pyrolysis temperature and the semicircle almost disappears at a high calcination temperature of 800 ° C, which indicates that the material prepared at a high temperature has a small charge transfer resistance. Moreover, the existence of the semicircle reflects that the as-obtained materials contain both pseudocapacitance and EDLC, which agrees well with the CV analysis and galvanostatic charge-discharge result. We have shown the equivalent circuit in the inset of Figure 7a and have modelled the corresponding circuit for the three types of carbons. The model fitting parameters are provided in the Table S2. The equivalent series resistance (ESR) including the resistance of electron/ion transfer. It is found that the ESR of NPLC-2 is smallest among all the samples, and its value is about 0.771 ohm. The slop of all the lines at medium-frequency region is nearly $45°$ and the length of NPLC-1 and NPLC-2 is shorter than that of NPLC-3, which indicates that the efficiency of electrolyte in NPLC-1 and NPLC-2 is higher when diffusing into pores. To describe the capacitive property more directly, Bode plot is shown in Fig. 7b. It can be observed that the phase angles of NPLC-2 and NPLC-3 are about $-87°$ and they are close to ideal value of full capacity of $-90°$. the relaxation time constant, τ_0 (the minimum time needed for all the energy to be discharged from the supercapacitor cell with an efficiency >50%), $\tau_0 = 1/2\pi f$, we can see from the Fig. 7b that $f_1 < f_2 < f_3$, so the relaxation time constant of NPLC-1 > NPLC-2 > NPLC-3, which means the NPLC-2 and NPLC-3 have the more appropriate pore size distribution for ions to transport. At whole analysis from EIS test, the performance of

NPLC-2 is superior to that of NPLC-1 and NPLC-3. In conclusion, its excellent electrochemical performance is benefited from the collaboration effect of 3D interconnected porous structure with different levels of pores, introduced nitrogen atoms and large surface area.

Conclusions

In this work, we successfully obtained 3D N-doped hierarchical porous lamellar carbon from mantis shrimp shell using a facile KOH activation method . The samples exhibits a high surface area, definite nitrogen atom percentage and an ideal hierarchical pore size distribution, including numerous micropores, the small mesopores and the relatively big mesopores.The rational structure of the material lead to outstanding electrochemical property used for supercapacitor: a high specific capacitance of 312.62 F g^{-1} at 0.3 A g^{-1}; as indicatedby a residual capacitance of 272.56 F g^{-1} at 20.0 A $g^{-1}$and a considerably superior cycling durability with a high capacitance retention of 96.26% after 10000 charge-discharge cycles. Moreover, the obtained sample presents high energy density and power density. The energy density of NPLC-2 can reach 10.12 Wh Kg^{-1} even at a large power density of 14580 W Kg^{-1} in a symmetrical two-electrode system in 6 M KOH solution. The excellent electrochemical performance is owing to the synergistic effect of 3D web-like porous lamellar porous structure with required moderate pore size distribution, high nitrogen doping content and satisfied surface area. The hierarchical porous stracture can provide open routes for rapid ion diffusion as well as storage bank of electrolyte ions for seasonable supplement of charges. Such result can give us certain inspiration and references as to design and optimize the structure of porous carbon electrode material for supercapacitor.

Acknowledgements

Notes and references

1 Y. Zhai, Y. Dou, D. Zhao and S. Dai, Adv. Mater., 2011, **23**, 4828.
2 J. Wang and S. Kaskel, J. Mater. Chem., 2012, **22**, 23710.
3 B. Xu, S.S. Hou, G.P. Cao and F. Wu, J. Mater. Chem., 2012, **22**, 19088.
4 L.L. Zhang, Y. Gu and X.S. Zhao, J. Mater. Chem. A, 2013, **1**, 9395.
5 M. Sevilla, W. Gu and G. Yushin, J. Power Sources, 2014, **267**, 26.
6 J. Xu, R. Zhang, P. Chen and S. Ge, J. Power Sources, 2014, **246**, 132.
7 Y. Tan, Q. Xie and N. Zheng, ACS Appl. Mater. Interfaces, 2013, **5**, 2241.
8 M. Li and J. Xue, J. Phys. Chem. C, 2014, **118**, 2507.
9 Y. Su, H. Jiang and J. Chen, J. Power Sources, 2014, **265**, 246.
10 R.L. Liu, W.J. Ji and Z.Q. Zhang, Carbon, 2014, **76**, 84.
11 Z. Li, Z. Xu, H. Wang and D. Mitlin, Energy Environ. Sci., 2013, **6**, 871.
12 J. McKittrick, P.Y. Chen, L. Tombolato, E.E. Novitskaya and Hirata, Mater. Sci. Eng. C, 2010, **30**, 331.
13 G.S. Sailaja, K. Sreenivasan and H.K. Varma, Acta Biomater., 2009, **5**, 1647.
14 W. Huang, H. Zhang, Y. Huang and W. Wang, Carbon, 2011, **49**, 838.
15 L. Sun, C.G. Tian, M.T. Li and H.G. Fu, J. Mater. Chem. A, 2013, **1**, 6462.
16 Y.S. Yun, J. Shim and H.J. Jin, RSC Adv., 2012, **2**, 4353.
17 C. Wu, X. Wang and B. Ju, J. Power Sources, 2013, **227**, 1.
18 J. Lu, L. Yang, B, Xu and X. Wang, ACS Catal., 2014, **4**, 613.
19 B. Xu, D. Zheng and M. Jia, Electrochim. Acta, 2013, **98**, 176.
20 C. Wang, G. Shao, Z. Ma and S. Liu, Electrochim. Acta, 2014, **130**, 679.
21 R.J. White, M. Antonietti and M.M. Titirici, J. Mater. Chem., 2009, **19**, 8645.
22 H. Guo and Q. Gao, J. Power Sources, 2009, **186**, 551.
23 J. Xu, C. Wu and S. Ge, Microporous and Mesoporous Mater., 2014, **198**, 74.
24 M.H. Ryu, K.N. Jung and S. Yoon, J. Phys. Chem. C, 2013, **117**, 8092.
25 T. Otowa, R. Tanibata and M. Itoh, Gas Sep. Purif., 1993, **7**, 241.
26 M. Li, J. Ding and J.M. Xue, J. Mater. Chem. A, 2013, **1**, 7469.
27 K.S. Xia, Q.M. Gao, J.H. Jiang and J. Hu, Carbon, 2008, **46** 1718.
28 P. Hao, Z.H. Zhao, Y.H. Leng, C.P. Wong, H. Liu and B.Yang, Nano energy, 2015, **15**, 9.
29 S.T. Navale, G.D. Khuspe, M.A. Chougule and V.B. Patil, J. Phys. Chem.Solids, 2014, **75**, 236.
30 A. Kumar, R.K. Singh, H.K. Singh and P. Srivastava, J. Power Sources, 2014, **246**, 800.
31 M. Zhou, F. Pu and S.Y. Guan, Carbon, 2014, **68**, 185.
32 L.P. Wang, Y. Zhou and J.S. Qiu, Microporous and Mesoporous Mater., 2013, **174**, 67.
33 W.J. Qian, F.X. Sun, Y.H. Xu and F. Yan, Energy Environ. Sci., 2014, **7**, 379.
34 Y.R. Liang, F.X. Liang, H. Zhong and D.C. Wu, J. Mater. Chem. A, 2013, **1**, 7000.
35 W. Xing, S.Z. Qiao, R.G. Ding and G.Q. Lu, Z.F. Yan, Carbon, 2006, **44**, 216.

RSC Advances Accepted Manuscript